J Nanopart Res (2016) 18:54
DOI 10.1007/s11051-016-3364-7

RESEARCH PAPER

Self-assembled peptides for coating of active sulfur nanoparticles in lithium–sulfur battery

Yead Jewel · Kisoo Yoo · Jin Liu · Prashanta Dutta

Received: 9 October 2015 / Accepted: 9 February 2016 / Published online: 19 February 2016

Abstract Development of lithium–sulfur (Li–S) battery is hindered by poor cyclability due to the loss of sulfur, although Li–S battery can provide high energy density. Coating of sulfur nanoparticles can help maintain active sulfur in the cathode of Li–S battery, and hence increase the cyclability. Among myriad of coating materials, synthetic peptides are very attractive because of their spontaneous self-assembly as well as electrical conductive characteristics. In this study, we explored the use of various synthetic peptides as a coating material for sulfur nanoparticles. Atomistic simulations were carried out to identify optimal peptide structure and density for coating sulfur nanoparticles. Three different peptide models, poly-proline, poly(leucine–lysine) and poly-histidine, are selected for this study based on their peptide–peptide and peptide-sulfur interactions. Simulation results show that both poly-proline and poly(leucine–lysine) can form self-assembled coating on sulfur nanoparticles (2–20 nm) in pyrrolidinone, a commonly used solvent for cathode slurry. We also studied the structural integrity of these synthetic peptides in organic [dioxolane (DOL) and dimethoxyethane (DME)] electrolyte used in Li–S battery. Both peptides show stable structures in organic electrolyte (DOL/DME) used in Li–S battery. Furthermore, the dissolution of sulfur molecules in organic electrolyte is investigated in the absence and presence of these peptide coatings. It was found that only poly(leucine–lysine)-based peptide can most effectively suppress the sulfur loss in electrolyte, suggesting its potential applications in Li–S battery as a coating material.

Keywords Synthetic peptides · Sulfur coating · Molecular simulation · Sulfur dissolution · Modeling and simulation · Energy storage

Introduction

In the last decade, Li-ion batteries have revolutionized the portable electronics market. Due to high energy and power density, the Li-ion batteries are widely used in various electronic devices such as laptops, cellphones, and tablets. However, even when fully developed, the highest energy storage achieved by a state-of-the-art Li-ion battery is still too low to meet current demands in the automotive industry, such as in electric vehicles and hybrid electric vehicles. For instance, the highest energy storage capability of current Li-ion battery is

Yead Jewel and Kisoo Yoo contributed equally to this work.

Electronic supplementary material The online version of this article (doi:10.1007/s11051-016-3364-7) contains supplementary material, which is available to authorized users.

Y. Jewel · K. Yoo · J. Liu · P. Dutta (✉)
School of Mechanical and Materials Engineering, Washington State University, Pullman, WA 99164-2920, USA
e-mail: prashanta@wsu.edu

~200 Wh/kg at cell-level and the driving range of a typical electric vehicle is less than 200 miles using Li-ion battery. Therefore, there is an increasing demand for light weight and high capacity batteries for next generation electric vehicles. Among various possible options, lithium–sulfur (Li–S) battery has the potential to transform the battery technology and can potentially replace the Li-ion battery since Li–S battery offers much higher theoretical specific energy (1672 mAh/g) (Bruce et al. 2012). The improvement on the specific energy is due to the fact that sulfur is used as active cathode material rather than heavy materials such as lithium cobalt oxide, lithium nickelate, and lithium manganite. In spite of the high energy density, the development of Li–S battery as a commercial product has been hindered by the short cycle life. The primary reason for low cyclability is the loss of active sulfur in most organic electrolyte solutions resulting from the dissolution of polysulfides (Song et al. 2013).

To improve the cycle life, a wide variety of cathodes have been investigated to constrain the active sulfur within cathode side (Ji et al. 2009; Liang et al. 2009; Moon et al. 2013; Xin et al. 2012; Zhao et al. 2013). In a seminal work, Ji et al. (Ji et al. 2009) reported that conductive mesoporous carbon framework (CMK-3) can constrain sulfur within its channel and maintain intimate electrical contact. In their experimental work, they have shown reversible capacity up to 1320 mAh/g. Later, Zhao et al. (2013) introduced graphene coating on the CMK-3 to enforce the sulfur trapping, which improved the cyclability. A number of other studies suggested encapsulation of sulfur before placing them to the electrically conductive porous materials. For instance, Li et al. (2013) coated the sulfur with polymer shell of polyvinyl pyrrolidone (PVP). These PVP-encapsulated sulfur nanospheres successfully reduced the polysulfide dissolution into electrolyte leading to superior cyclic performance of Li–S battery. However, the poor electrical conductivity of PVP was an issue for Li–S battery. Later Chen et al. (Chen et al. 2013) reported an improvement by polymerizing 3,4-ethylene dioxythiophene (EDOT) into the PVP to increase the electrical conductivity of PVP. Even though EDOT can introduce conductive characteristic on PVP coating, the polymerization process is very complex as it requires extra synthesis steps involving mixing, polymerization, separation, rinsing, etc. Thus, there is a critical need for the development of coating materials for sulfur nanoparticles, which is inherently conductive for electrons.

In this study, an innovative sulfur coating mechanism is proposed using synthetic peptides. Peptides have many attractive characteristics as a sulfur encapsulation material for Li–S batteries. First, the electrical conductivity of self-assembled peptide can be tailored by selecting electrically conductive peptides as well as doping electrically conductive materials (Nalluri et al. 2014; Scheibel et al. 2003; Xu et al. 2010). Second, as a self-assembled biomolecule, peptide structures can be manipulated to form various configurations, such as sheet, fiber, and sphere (Fairman and Akerfeldt 2005; Krebs et al. 2007), such that the self-assembled peptides can be used to coat different shapes of active materials (e.g., sulfur nanoparticle, S/CMK-3, and sulfur-carbon fiber). Considering the aforementioned favorable properties of peptides, the main objective of this study is to design the optimal peptide chains that can be self-assembled on sulfur nanoparticles for high-performance Li–S battery. We used molecular dynamic simulations to show the interactions between (i) sulfur and peptide and (ii) peptide and peptide, and the formation of self-assembled peptide-coated sulfur nanoparticles. Furthermore, we studied the dissolution rate of sulfur into the electrolyte in the presence and absence of peptide coatings to demonstrate the effectiveness of selected peptide coatings.

Method

Design of synthetic peptides as coating materials

Although sulfur nanoparticles (~200 nm) can be obtained from simple reaction between sodium thiosulfate and hydrochloric acid (Li et al. 2013), these particles need to be encapsulated within coating materials to avoid rapid dissolution in organic electrolytes (e.g., DOL/DME). If the rate of sulfur solvation is much higher than the reduction rate due to reactions in the cathodic side, sulfur molecules will move to the anodic side, causing reduction reactions at the anode resulting in rapid loss of sulfur as well as power. This loss of active sulfur is directly responsible for poor cyclability of a Li–S battery. In this study, we explore the use of synthetic peptides as a new coating material to reduce rapid dissolution of sulfur in organic electrolytes. Figure 1 illustrates the overall coating process of sulfur nanoparticles with synthetic

peptide molecules. For effective encapsulation of sulfur nanoparticles, the peptides should possess some special characteristics: First, the peptides should interact strongly with sulfur molecules as well as other peptides in a solution to form peptide-coated sulfur nanoparticle. Second, the assembled peptide layer configuration should be strong enough to maintain its structure in electrolytes of Li–S battery. Third, the coating layer should be electrically conductive to transfer electrons to sulfur for cathodic reactions.

Electrically conductive peptides can be designed based on the proper selection of amino acids to donate, relay, and accept electrons. Tyrosine is most widely used as an electron donor, and it can be found in most proteins in neutral form (Reece et al. 2006; Stubbe and van der Donk 1998). Cationic radicals, such as tryptophan (Shafaat and Kim 2014) and dialkoxyphenyl (Gao et al. 2011) are the best choices for electron acceptor since they can inject a net positive charge to their adjacent amide groups. The role of relay is to transfer electrons from donor to acceptor using its amide groups. Proline is mostly used as relay in amino acid (Lauz et al. 2012). Other possible choices for relay amino acids are glycine, lysine, glutamic acid (Faraggi et al. 1989), and leucine-Aib(α-aminoisobutyric acid) (Kitagawa et al. 2003).

In our study, we have considered three electrically conductive synthetic peptides with tyrosine (Tyr) and radical tryptophan (Trp*) as the electron donor and acceptor, respectively. In the first peptide (Tyr-$(Pro)_6$-Trp* or PP), as shown in Fig. 2a, proline (Pro) is used as a relay amino acid, and Tyr is added to N-terminus of the peptide, and Trp* is added to C-terminus of the peptide. Experimental studies have demonstrated very good electrical conductivity for this synthetic peptide (Lauz et al. 2012), but the self-assembly characteristics of this peptide is not known yet. In the second peptide (Tyr-$(Leu\text{-}Lys)_3$-Trp* or LK), as shown in Fig. 2b, leucine (L)–lysine (K) are the relay amino acids. This peptide can form beta sheet amyloid fibrils (Rufo et al. 2014) in polar solvent due to the periodic arrangement of polar (K) and non-polar (L) groups. The amyloid fibrils can help cover any surface. In the third peptide, we also considered a short alpha-helix peptide (Tyr-$(His)_6$-Trp* or HH) with 6 histidine amino acids as illustrated in Fig. 2c. In this peptide, the π-stacking interactions between imidazole groups lead to strong peptide–peptide interactions. All three peptides are attractive to the sulfur surface because of the nitrogen atoms on backbone of PP, side chain K of LK and side chain H of HH peptides. The tyrosine and radical tryptophan have been added as electron donor and acceptor in all peptides to improve their electron conductivities; however, during the battery operations, the fast oxidation/reduction reactions may cause the electrochemical stability issues of tyrosine and tryptophan radicals. The tyrosine radicals are stable for days at room temperature (Wallar and Lipscomb 1996), but the lifetime of tryptophan radicals span a wide range from microseconds to seconds in biological systems (Aubert et al. 2000; Deligiannakis and Rutherford 2001; Krebs et al. 2000). We expect that the radicals are more stable in a non-aqueous environment, but the local electrostatic field and

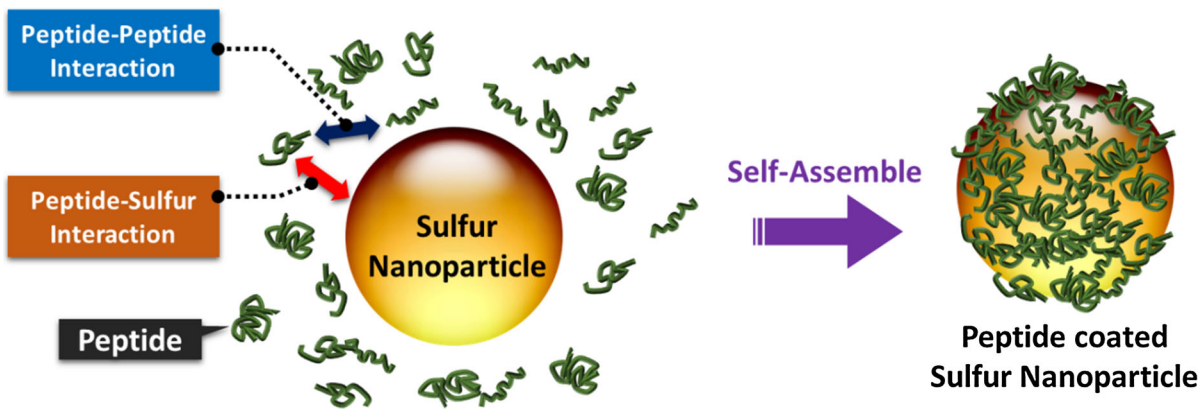

Fig. 1 Schematic of key interactions for formation of peptide self-assembly on a sulfur nanoparticle. The peptide coating formed on active sulfur should be able to mitigate the dissolution of sulfur into organic electrolytes

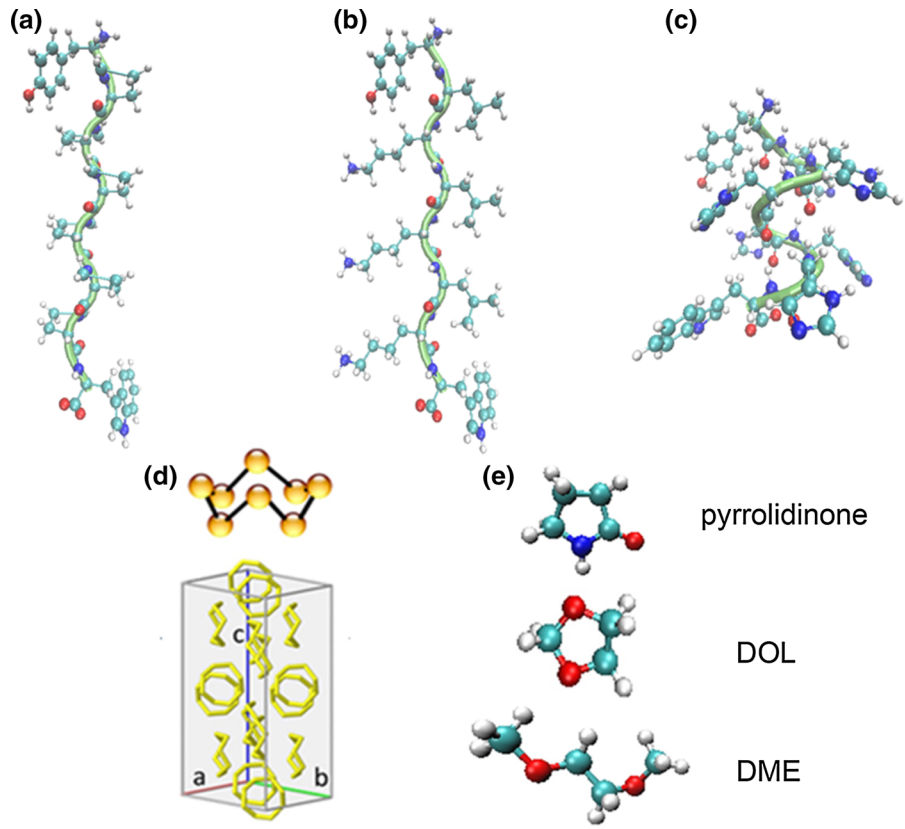

Fig. 2 Ball and stick models for (**a**) **PP** (Tyr-$(Pro)_6$-Trp*), (**b**) **LK** (Tyr-$(Leu\text{-}Lys)_3$-Trp*) and (**c**) **HH** (Tyr-$(His)_6$-Trp*). (**d**) α-S_8 crown shaped octa-sulfur (*yellow*) and the unit cell of the orthorhombic crystal structure. Although sulfur has 30 well-characterized solid allotropes depending on preparation conditions such as pressure and temperature, α-S_8 is the only stable form of sulfur that can form orthorhombic crystal structure in most solvents. (**e**) The ball and stick models for solvent/electrolyte molecules. (Color figure online)

transport of lithium ions during Li–S battery operations may greatly impact their stability. Further experiments and density function theory (DFT) calculations are needed to address the electrochemical stability issue of these radicals in Li–S battery environment, which is beyond the scope of this paper and will not be discussed further.

Active cathode material-octa-sulfur

Sulfur, the active cathode materials for Li–S battery, has 30 well-characterized solid allotropes depending on preparation conditions such as pressure and temperature. Among them there are three cyclo-octa-sulfurs (S_8) varying in crystal structures. α-S_8 is the only stable form of sulfur under standard temperature and pressure, and it can form orthorhombic crystal structure in most solvents (Steudel and Eckert 2003). The other two octa-sulfur (monoclinic β-S_8 and γ-S_8) crystal structures are unstable at room temperature. β-S_8 is stable above 96 °C, and γ-S_8 is metastable in all temperature and occasionally crystallizes. Thus, in our simulations, we will use α-S_8 crystals as the active cathode materials for Li–S battery. The crystal structure of α-S_8 is shown in Fig. 2d.

Simulation details

Molecular dynamics (MD) simulations were performed using NAMD version 2.9 (Phillips et al. 2005). The peptides were modeled using VMD (Humphrey et al. 1996), and the charges of the peptide atoms and missing hydrogen atoms were reassigned using VMD psfgen program. The CHARMM force field was used for peptides (Best et al. 2012); for octa-sulfur (α-S_8, the active cathode materials) and solvent/electrolytes, we used the CGENFF (CHARMM generalized force field (Vanommeslaeghe and MacKerell 2012; Vanommeslaeghe et al. 2012)). Charges of the tryptophan radicals are obtained according to Bernini et al. (Bernini et al. 2011), in which the electron paramagnetic resonance parameters of tyrosine and tryptophan were calculated from density

functional theory. Periodic boundary conditions were applied in all directions. The long-range electrostatic interactions were treated using particle mesh Ewald (PME) method, and the van der Waals interactions were calculated using Lennard-Jones potential with a cut-off of 10 Å. To prepare the solvents (pyrrolidinone and DOL/DME), solvent molecules were initially placed randomly in a large box, and energy-minimization NPT simulations were performed at 300 K and 1 atm until the volume of the system stayed constant. In our simulations, the orthorhombic crystal structure (Fig. 2d) of α-S_8 was obtained from the initially randomly distributed sulfur molecules in pyrrolidinone solvent; the sulfur molecules self-assembled into different shapes depending on the mole fraction during NPT simulations. Once orthorhombic α-S_8 was formed, different peptides were introduced to form self-assembled coating structure. Then, the pyrrolidinone solvent was replaced by an organic electrolyte, a mixture of DOL and DME, to study the integrity of the peptide coating materials as well as the dissolution of sulfur into the electrolyte. The molecular structures of different solvent and electrolyte molecules are illustrated in Fig. 2e. For all simulations, the production NPT runs were performed at room temperature ($T = 300$ K) and atmospheric pressure with time step of 2 fs. The SHAKE algorithm (Andersen 1983) was implemented for all the hydrogen atoms, and the multiple time stepping algorithm was used for long-range electrostatic interactions. Simulation box sizes were maintained $\sim$64 Å $\times$ 64 Å $\times$ 64 Å unless otherwise mentioned.

Results

Sulfur structure

To obtain crystal structure of octa-sulfur (α-S_8) in organic pyrrolidinone solvent, we conducted two different studies in the same box size ($\sim$70 Å $\times$ 70 Å $\times$ 70 Å) by changing the number of randomly distributed octa-sulfur molecules. Figure 3a shows the spherical shape sulfur nanoparticle (yellow color) formed from 77 sulfur molecules. The sulfur molecules form a plate as the number increases to 376 (Fig. 3b). In both cases, the orthorhombic crystal structure is achieved as shown in Fig. 3c. From our results, we calculated the α-S_8 crystal structural parameters (the rectangular base a, b, and height c in the rectangular prism as shown in Figs. 2d and 3c) and compared with the experimental data. Table 1 lists the average values of crystal structure parameters and the sulfur density. The predicted results agree with the experimental measurements from the X-ray crystallography analysis (Rettig and Trotter 1987).

Self-assembly of peptides on sulfur nanoparticles

To investigate the assembly of peptides on sulfur surface, we considered three different synthetic peptides (LK, PP, and HH) in pyrrolidinone as described before. A plate of solid sulfur with thickness of $\sim$1.8 nm was cut from the solid sulfur in Fig. 3b, and then the sulfur molecules were constrained to their equilibrium positions with a harmonic force in all directions mimicking a solid sulfur surface. Then 32 peptides were randomly distributed in the pyrrolidinone solvent, and MD simulations were performed until the peptides assemble on the sulfur plate and equilibrium structures were formed. After that, the pyrrolidinone solvent was replaced with DOL/DME electrolyte; simulations were continued until equilibrium state was reached in DOL/DME. Figure 4 illustrates the snapshots of initial and final stages of the assembly process for various peptides in different solutions.

Figure 5 shows the peptide distribution near the sulfur surface for all three peptides in pyrrolidinone solvent as well as in DOL/DME electrolyte. For both LK and PP models (Fig. 5a, b), the peptides self-assembled onto the sulfur surface in pyrrolidinone due to the attractive interactions between nitrogen atoms and sulfur molecules. As pyrrolidinone was replaced by the DOL/DME electrolyte, the peptides were stably distributed and even came closer to the sulfur surface. This is due to the fact that the oxygen atom on DME molecule is able to form hydrogen bond with the CH_3 groups on LK model and CH_2 groups on PP model (see Fig. 2), while the other side of DME molecule binds strongly to the solid sulfur surface via oxygen and CH_n ($n = 2$ or 3) groups. Therefore, the DME molecules act as a link between the sulfur surface and CH_n ($n = 2$ or 3) groups on peptides which are originally away from the sulfur, and bring peptides closer to sulfur. This effect is more pronounced for PP model because its side chains are much shorter than LK

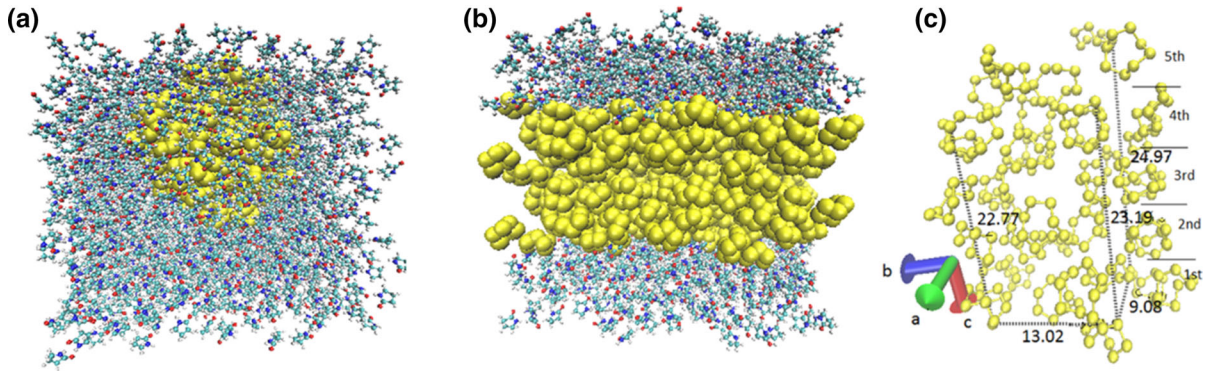

Fig. 3 Sulfur (a) ball and (**b**) plate (*yellow color*, VDW representation) formation in pyrrolidinone solvent. The number of sulfur molecules used in cases (**a**) and (**b**) are 77 and 376, respectively. (**c**) Calculation of unit cell parameters (**a**, **b** and **c**) of octa-sulfur crystal structure by taking the second atom of sulfur ring (see Fig. 2d) as a reference point. Five layers of sulfur are shown to compare with the orthorhombic crystal structure presented in Fig. 2d. (Color figure online)

Table 1 Properties of orthorhombic crystal structure of α-S_8. The numerical results are based on the average over three independent simulations

	a (Å)	b (Å)	c (Å)	ρ (g/cm^3)
Molecular simulation	10.46	12.87	24.49	1.97
Experimental results (Rettig and Trotter 1987)	10.21	12.14	24.67	2.07

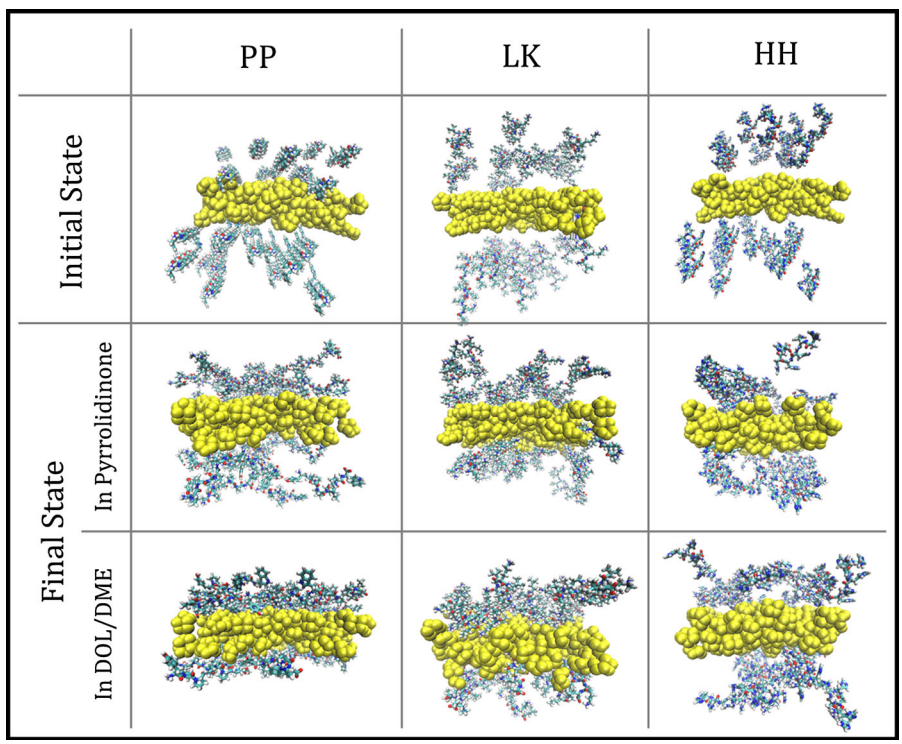

Fig. 4 Formation of coated layer on sulfur surface due to self-assembly of peptides. All peptides assembled on the sulfur surface. PP peptides distributed more uniformly due to weak peptide–peptide interactions, while LK peptides partially agglomerate and HH peptides form large agglomeration due to strong peptide–peptide interactions

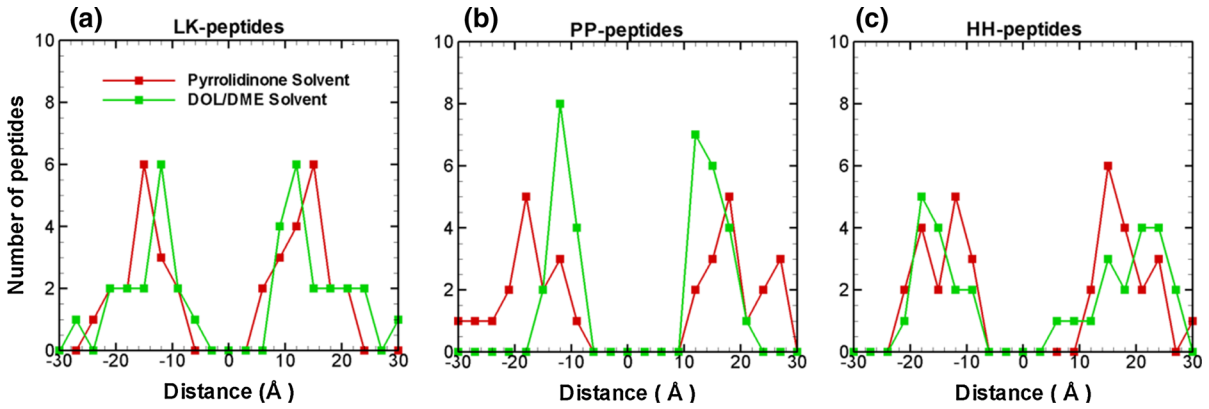

Fig. 5 Peptide distribution in pyrrolidinone solvent (*red*) and DOL/DME electrolyte (*green*) for (**a**) LK model, (**b**) PP model and (**c**) HH model on both sides of the sulfur plate. The numbers of peptides at different locations were calculated using a bin size of 3 Å and averaged over 10 ns after equilibrium. (Color figure online)

model as shown in Fig. 2. For HH peptides, as shown in Fig. 5c, peptides are attracted onto sulfur surface, and different solutions do not have much effect on the peptide distribution. However, as illustrated in Fig. 4 (for HH), the strong peptide–peptide interactions (from the π-stacking interactions) cause large agglomerations of peptides. As a consequence, the HH peptides cannot effectively cover the sulfur surface, and we will only consider LK and PP models for the rest of the study.

Sulfur dissolution in electrolytes

Next we investigate the dissolution of solid sulfur in DOL/DME electrolytes in the presence and absence of peptide coatings. In our simulations, 77 sulfur molecules were initially placed randomly and formed a solid sulfur sphere in pyrrolidinone solvent, and then 39 peptides (LK and PP models) were added into the solution to cover the sulfur surface (see Supporting materials). After that the pyrrolidinone was replaced by DOL/DME electrolyte, and we track the number of sulfur molecules dissolved into the solution as a function of simulation time. Figure 6a shows the dissolution of solid sulfur in electrolyte for different cases with and without peptides' coating.

In each case, we have performed three independent simulations, but they produced similar results, and we only show one result for each case in Fig. 6. As shown in Fig. 6a and illustrated in the corresponding snapshot in Fig. 6b, the sulfur rapidly dissolved into DOL/DME without peptide coating, and this finding is consistent with experimental observations. But the dissolution process is significantly reduced when the sulfur is coated with peptides (Fig. 6c, d). Comparing the results from LK and PP peptides' coating, the LK peptides are much more effective than PP peptides to slow down the sulfur dissolution. This is due to the stronger peptide–peptide interactions from the periodicity of the polar and non-polar groups in LK peptide assisting to form β-sheet in polar solvent (Xiong et al. 1995). These results suggest that one has to carefully tune the peptide–peptide interactions in designing a synthetic peptide for sulfur coating. If the peptide–peptide interactions are too strong, peptides form large agglomerates and cannot fully cover the sulfur surface (as in our HH peptide). While the peptide–peptide interactions are weak, the peptide coating is loose and cannot effectively prevent sulfur from dissolving. Among the peptides (LK, PP, HH) we considered in this study, LK peptide can be used as an effective coating materials in Li–S batteries to slow down the loss of active sulfur materials at the cathode side.

Conclusions

Molecular dynamics simulations were used to design a new sulfur coating material for Li–S batteries. Three different types of electrically conductive synthetic peptides were evaluated in this study. Six amino acids were used to design the relay part of each peptide along with tyrosine and radical tryptophan as the

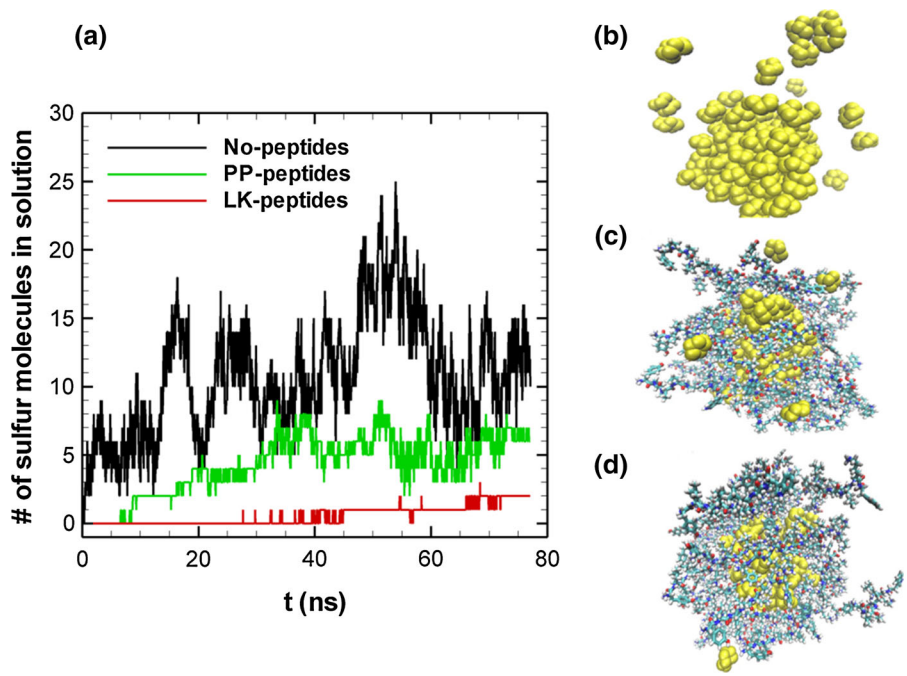

Fig. 6 (**a**) Dissolution of sulfur molecules in DOL/DME electrolyte as a function of simulation time under different conditions. Snapshots for sulfur (VDW representation in *yellow* color) dissolution in electrolyte, (**b**) without any peptide, (**c**) with 39 PP peptides, and (**d**) with 39 LK peptides at 75 ns. (Color figure online)

electron donor and acceptor, respectively. The relay part of the first and third peptides consists of proline and histidine, respectively, while alternate arrangement of leucine and lysine amino acids was used for the second peptide. Molecular dynamics results show that both poly-proline and poly(leucine–lysine) peptides can effectively cover the sulfur surface in both pyrrolidinone and DOL/DME solvents. On the other hand, alpha-helix peptides constructed from histidine form large agglomerates due to very strong peptide–peptide interactions, and this peptide cannot fully cover the sulfur surface. Molecular dynamics results also indicate that only poly(leucine–lysine) peptide can be used as an effective coating material to slow down the loss of active sulfur materials at the cathode side of a Li–S cell.

One potential concern of sulfur surface coating with peptides is its effect on the lithium ion diffusion across peptide layer. The exact effect is complicated due to the structural and compositional complexity of peptides. However, we have estimated the porosity ($\sim$0.4) and the average pore size ($\sim$1 nm) for the case with 39 LK peptides, and the pore size is much larger than the lithium ion size ($\sim$0.09 nm). Therefore, the peptide coating should not significantly hinder the diffusion of lithium ions if treated as a simple porous structure. Thus, the properly designed peptides may potentially be adopted as an alternative to replace the currently used coating materials. However, extensive work, including experiments and DFT calculations, is warranted to resolve the electrochemical stability issue between Li ion and conductive peptide before practical application of this biomaterial as coating in Li–S battery.

Acknowledgments This work was supported in part by the US National Science Foundation under Grant No. CBET 1250107.

References

Andersen HC (1983) Rattle-a velocity version of the shake algorithm for molecular-dynamics calculations. J Comput Phys 52:24–34

Aubert C, Vos MH, Mathis P, Eker APM, Brettel K (2000) Intraprotein radical transfer during photoactivation of DNA photolyase. Nature 405:586–590

Bernini C, Pogni R, Ruiz-Duenas FJ, Martinez AT, Basosia R, Sinicropi A (2011) EPR parameters of amino acid radicals in P. eryngii versatile peroxidase and its W164Y variant computed at the QM/MM level. Phys Chem Chem Phy 13:5078–5098

Best RB, Zhu X, Shim J, Lopes PEM, Mittal J, Feig M, MacKerell AD Jr (2012) Optimization of the Additive

CHARMM All-atom protein force field targeting improved sampling of the backbone phi, psi and side-chain chi(1) and chi(2) dihedral angles. J Chem Theory Comput 8:3257–3273

Bruce PG, Freunberger SA, Hardwick LJ, Tarascon JM (2012) Li-O-2 and Li–S batteries with high energy storage. Nat Mater 11:19–29

Chen H, Dong W, Ge J, Wang C, Wu X, Lu W, and Chen L (2013) Ultrafine sulfur nanoparticles in conducting polymer shell as cathode materials for high performance lithium/sulfur batteries. Scientific Reports *3*

Deligiannakis Y, Rutherford AW (2001) Electron spin echo envelope modulation spectroscopy in photosystem I. Biochim Et Biophys Acta-Bioenerg 1507:226–246

Fairman R, Akerfeldt KS (2005) Peptides as novel smart materials. Curr Opin Struct Biol 15:453–463

Faraggi M, Defelippis MR, Klapper MH (1989) Long-range electron-transfer between tyrosine and tryptophan in peptides. J Am Chem Soc 111:5141–5145

Gao J, Mueller P, Wang M, Eckhardt S, Lauz M, Fromm KM, Giese B (2011) Electron transfer in peptides: the influence of charged amino acids. Angew Chem-Int Ed 50:1926–1930

Humphrey W, Dalke A, Schulten K (1996) VMD: visual molecular dynamics. J Mol Graph Model 14:33–38

Ji X, Lee KT, Nazar LF (2009) A highly ordered nanostructured carbon-sulphur cathode for lithium–sulphur batteries. Nat Mater 8:500–506

Kitagawa K, Morita T, Kawasaki M, Kimura S (2003) Electric properties of self-assembled monolayers of helical peptides by scanning tunneling spectroscopy. J Polymer Sci Part A 41:3493–3500

Krebs C, Chen SX, Baldwin J, Ley BA, Patel U, Edmondson DE, Huynh BH, Bollinger JM (2000) Mechanism of rapid electron transfer during oxygen activation in the R2 subunit of Escherichia coli ribonucleotide reductase. 2. Evidence for and consequences of blocked electron transfer in the W48F variant. J Am Chem Soc 122:12207–12219

Krebs MRH, Devlin GL, Donald AM (2007) Protein particulates: another generic form of protein aggregation? Biophys J 92:1336–1342

Lauz M, Eckhardt S, Fromm KM, Giese B (2012) The influence of dipole moments on the mechanism of electron transfer through helical peptides. Phys Chem Chem Phys 14: 13785–13788

Li W, Zheng G, Yang Y, Seh ZW, Liu N, Cui Y (2013) High-performance hollow sulfur nanostructured battery cathode through a scalable, room temperature, one-step, bottom-up approach. Proc Natl Acad Sci USA 110:7148–7153

Liang C, Dudney NJ, Howe JY (2009) Hierarchically structured sulfur/carbon nanocomposite material for high-energy lithium battery. Chem Mater 21:4724–4730

Moon S, Jung YH, Jung WK, Jung DS, Choi JW, Kim DK (2013) Encapsulated monoclinic sulfur for stable cycling of Li-S rechargeable batteries. Adv Mater 25:6547–6553

Nalluri SKM, Shivarova N, Kanibolotsky AL, Zelzer M, Gupta S, Frederix PWJM, Skabara PJ, Gleskova H, Ulijn RV (2014) Conducting nanofibers and organogels derived from the self-assembly of tetrathiafulvalene-appended dipeptides. Langmuir 30:12429–12437

Phillips JC, Braun R, Wang W, Gumbart J, Tajkhorshid E, Villa E, Chipot C, Skeel RD, Kale L, Schulten K (2005) Scalable molecular dynamics with NAMD. J Comput Chem 26:1781–1802

Reece SY, Hodgkiss JM, Stubbe J, Nocera DG (2006) Proton-coupled electron transfer: the mechanistic underpinning for radical transport and catalysis in biology. Philosoph Trans R Soc B 361:1351–1364

Rettig SJ, Trotter J (1987) Refinement of the structure of orthorhombic sulfur, alpha-s-8. Acta Crystallogr Sect C 43:2260–2262

Rufo CM, Moroz YS, Moroz OV, Stoehr J, Smith TA, Hu X, DeGrado WF, Korendovych IV (2014) Short peptides self-assemble to produce catalytic amyloids. Nat Chem 6:303–309

Scheibel T, Parthasarathy R, Sawicki G, Lin XM, Jaeger H, Lindquist SL (2003) Conducting nanowires built by controlled self-assembly of amyloid fibers and selective metal deposition. Proc Natl Acad Sci USA 100:4527–4532

Shafaat HS, Kim JE (2014) Resonance Raman Analysis of the Tryptophan Cation Radical. J Phys Chem Lett 5:3009–3014

Song M-K, Cairns EJ, Zhang Y (2013) Lithium/sulfur batteries with high specific energy: old challenges and new opportunities. Nanoscale 5:2186–2204

Steudel R, Eckert B (2003) Solid sulfur allotropes. Elem Sulfur Sulfur-Rich Compd 230:1–79

Stubbe J, van der Donk WA (1998) Protein radicals in enzyme catalysis. Chem Rev 98:705–762

Vanommeslaeghe K, MacKerell AD Jr (2012) Automation of the CHARMM General Force Field (CGenFF) I: bond perception and atom typing. J Chem Inf Model 52:3144–3154

Vanommeslaeghe K, Raman EP, MacKerell AD Jr (2012) Automation of the CHARMM general force field (CGenFF) II: assignment of bonded parameters and partial atomic charges. J Chem Inf Model 52:3155–3168

Wallar BJ, Lipscomb JD (1996) Dioxygen activation by enzymes containing binuclear non-heme iron clusters. Chem Rev 96:2625–2657

Xin S, Gu L, Zhao N-H, Yin Y-X, Zhou L-J, Guo Y-G, Wan L-J (2012) Smaller sulfur molecules promise better lithium–sulfur batteries. J Am Chem Soc 134:18510–18513

Xiong HY, Buckwalter BL, Shieh HM, Hecht MH (1995) Periodicity of polar and nonpolar amino-acids is the major determinant of secondary structure in self-assembling oligomeric peptides. Proc Natl Acad Sci USA 92:6349–6353

Xu H, Das AK, Horie M, Shaik MS, Smith AM, Luo Y, Lu X, Collins R, Liem SY, Song A et al (2010) An investigation of the conductivity of peptide nanotube networks prepared by enzyme-triggered self-assembly. Nanoscale 2:960–966

Zhao XY, Tu JP, Lu Y, Cai JB, Zhang YJ, Wang XL, Gu CD (2013) Graphene-coated mesoporous carbon/sulfur cathode with enhanced cycling stability. Electrochim Acta 113:256–262